Lab on a Chip

PAPER

View Article Online
View Journal | View Issue

Cite this: *Lab Chip*, 2014, **14**, 547

A digital microfluidic electrochemical immunoassay

Mohtashim H. Shamsi,†[ab] Kihwan Choi,†[ab] Alphonsus H. C. Ng[bc] and Aaron R. Wheeler*[abc]

Received 18th September 2013,
Accepted 13th November 2013

DOI: 10.1039/c3lc51063h

www.rsc.org/loc

Digital microfluidics (DMF) has emerged as a popular format for implementing quantitative immunoassays for diagnostic biomarkers. All previous reports of such assays have relied on optical detection; here, we introduce the first digital microfluidic immunoassay relying on electrochemical detection. In this system, an indium tin oxide (ITO) based DMF top plate was modified to include gold sensing electrodes and silver counter/pseudoreference electrodes suitable for in-line amperometric measurements. A thyroid stimulating hormone (TSH) immunoassay procedure was developed relying on magnetic microparticles conjugated with primary antibody (Ab_1). Antigen molecules are captured followed by capture of a secondary antibody (Ab_2) conjugated with horseradish peroxidase enzyme (HRP). HRP catalyzes the oxidation of 3,3′,5,5′-tetramethylbenzidine (TMB) which can be detected amperometrically. The limit of detection of the technique (2.4 μIU mL^{-1}) is compatible with clinical applications; moreover, the simplicity and the small size of the detector suggest utility in the future for portable analysis.

Introduction

Digital microfluidics (DMF) is a state-of-the-art liquid-handling technology that manipulates fluids as discrete droplets on open surfaces.[1–7] DMF devices comprise an open array of electrodes covered with a hydrophobic insulator. When electric potentials are applied to the electrodes, electrostatic forces are generated, which can be made to cause droplets to move, merge, mix, split, and dispense from reservoirs. DMF permits assay development with low reagent consumption and allows for facile integration with analytical techniques. Moreover, the simple and compact design inherent to DMF is useful for parallel implementation of different processes.[8] These characteristics make DMF suitable for applications ranging from cell culture and assays[9–13] to DNA and protein processing and analysis.[14–21]

The unique characteristics of DMF make it particularly well suited for implementing miniaturized immunoassays.[22–28] In these systems, sample droplets containing antigens are dispensed from reservoirs and then exposed to antibodies immobilized on the device surface[22] or on beads[23–28] to separate the antigens from other sample constituents. In all examples published previously, the detection mode for DMF-enabled immunoassays has been optical (*i.e.*, fluorescence[22,24,25,27] or chemiluminescence[23,26,28]). Optical detection methods are a standard work-horse for laboratory work, but electroanalytical techniques are becoming popular for immunoassays because of the potential for low-cost, sample volume-independent output,[29] particularly for applications requiring miniaturized/portable analysis systems. The format of digital microfluidic devices, which inherently comprise an array of electrodes, seems to be a good match for electroanalytical immunoassays (or "electroimmunoassays"), but to our knowledge, this has never been reported previously.

There have been only a few reports describing the marriage of digital microfluidics and electrochemical detection.[30–34] None of these techniques were applied to immunoassays, and in addition, most of these initial reports (with one exception[34]) either lack detailed electrochemical characterization or used external electrodes for measurements. Here, we introduce the first digital microfluidic electroimmunoassay. The electroanalysis system is integrated into the device top plate, with each system bearing a dedicated gold working electrode (WE) and a silver counter/pseudoreference (CE/RE) electrode. This method was characterized and applied to on-chip detection of thyroid stimulating hormone (TSH) in a "sandwich" type immunoassay

[a] *Department of Chemistry, University of Toronto, 80 St George St., Toronto, ON, M5S 3H6, Canada. E-mail: aaron.wheeler@utoronto.ca; Fax: +1 (416) 946 3865; Tel: +1 (416) 946 3864*
[b] *Donnelly Centre for Cellular and Biomolecular Research, 160 College St., Toronto, ON, M5S 3E1, Canada*
[c] *Institute of Biomaterials and Biomedical Engineering, University of Toronto, 164 College St., Toronto, ON, M5S 3G9, Canada*
† These authors contributed equally.

by amperometry. We propose that this system (and variations thereof) will be useful for a wide range of applications in the future.

Experimental

Materials and methods

Unless otherwise specified, general-use reagents were purchased from Sigma Chemical (Oakville, ON, Canada) or Fisher Scientific Canada (Ottawa, ON, Canada). Analytical grade reagents were used to make aqueous solutions of 2.0 mM $KAuCl_4$ in 0.5 M H_2SO_4, 0.3 M $AgNO_3$ in 3 M NH_4OH, 1 mM $K_3Fe(CN)_6$, 0.2 M Na_2HPO_4, and 0.1 M citric acid ($C_6H_8O_7$). The latter two were mixed 4.6 : 1 to form McIlvaine's buffer with pH 7.0. Thyroid stimulating hormone (TSH) standard solutions and diluents (proprietary mixtures including TRIS and protein stabilizers) and Anti-β TSH coated paramagnetic microparticles were from ARCHITECT immunoanalyzer reagent kits (7K62) obtained from Abbott Laboratories (Abbott Park, IL).

Six custom immunoassay solutions/suspensions were formed for use on DMF devices. Briefly, (1) Ab_1 microparticle suspension was formed by immobilizing, washing and resuspending the particles at ~3.0×10^8 mL^{-1} in Tris-base (6.1 g L^{-1}), NaCl (5.8 g L^{-1}), BSA (1% w/v), and thimerosal (0.05% w/v). (2) Ab_2–HRP solution was formed by dissolving horse-radish peroxidase (HRP) conjugated mouse monoclonal Anti-TSH from Abcam (Cambridge, MA) at various concentrations in Tris-base (1.9 g L^{-1}), Tris–HCl (13.2 g L^{-1}), NaCl (17.5 g L^{-1}), BSA (1% w/v), cold fish gelatin (0.1% w/v), and thimerosal (0.05% w/v). (3) Wash buffer (pH 7.7) was formed from Tris-base (0.35 g L^{-1}), Tris–HCl (1.10 g L^{-1}), and NaCl (8.367 g L^{-1}). (4) TSH samples were formed by mixing 0 μIU mL^{-1} and 40 μIU mL^{-1} TSH standards at appropriate ratios. (5) Stable peroxide substrate buffer and 3,3′,5,5′-tetramethylbenzidine (TMB) substrate were purchased from Thermo Scientific (Rockford, IL). (6) Stop solution was adapted from TSH well-plate ELISA kits from Calbiotech (Spring Valley, CA). All six solutions/suspensions were supplemented with Pluronic L64 (0.05% v/v) prior to use.

Fabrication of DMF bottom-plates

Digital microfluidic device bottom plates were fabricated in the Toronto Nanofabrication Centre (TNFC) cleanroom facility. Chromium-on-glass substrates (coated with Parylene-C and Teflon-AF) were identical to those reported previously,[26] featuring an array of 80 chromium actuation electrodes (2.2 × 2.2 mm ea.) connected to 8 reservoir electrodes (16.4 × 6.7 mm ea.) and 4 waste reservoir electrodes (16.4 × 6.4 mm ea.). The actuation electrodes were roughly square with interdigitated borders (140 μm peak to peak sinusoids) and inter-electrode gaps of 30–80 μm.

Fabrication of DMF top-plates

Top-plates of DMF devices were formed from indium–tin oxide (ITO) coated glass substrates (Delta Technologies Ltd, Stillwater, MN) in three stages. In the first stage, the substrates were sonicated in acetone for 5 min and rinsed in 2-propanol for 1 min. After drying and dehydrating, substrates were spin-coated (3000 RPM, 45 s) with Shipley S1811 photoresist (Marlborough, MA) and then post-baked on a hot plate (95 °C, 2 min). Subsequently, the substrates were exposed (29.8 mW cm^{-2}, 10 s) through a mask. The substrates were developed for 3 min by immersing in MF-321 (MicroChem, Newton, Massachusetts), post-baked on a hot plate (125 °C, 1 min), and then etched for 10 min by immersing in ITO etchant comprising 4 : 2 : 1 (v/v/v) hydrochloric acid, deionized (DI) water, and nitric acid. After rinsing, the remaining photoresist was stripped for 5 min by immersing in AZ300T (Capitol Scientific Inc., Texas). When complete, the ITO on the device was separated into seven isolated regions, including six electroanalysis electrodes (four 1.6 mm diameter circles and two 1.2 × 1.2 mm squares) and one large, irregularly shaped DMF driving electrode. Each electroanalysis electrode was connected to a contact pad on the edge of the substrate.

In the second stage, a spin-coat/lift-off process described in detail elsewhere[11] was used to apply a patterned coating of Teflon-AF to the surface of the patterned ITO. When complete, the surface was globally coated with Teflon-AF with six apertures, one positioned over each of the electroanalysis electrodes (circular apertures with diameters of 0.6, 0.8, 1.0 or 1.2 mm over the circular electrodes and 0.4 × 0.4 mm square apertures over the square electrodes).

In the third stage, gold or silver was electrodeposited onto the electroanalysis electrodes through the apertures in the Teflon-AF. A 20 μL aliquot of plating solution (2.0 mM $KAuCl_4$ in 0.5 M H_2SO_4 for gold and 0.3 M $AgNO_3$ in 3 M NH_4OH for silver) was deposited onto the electroanalysis electrodes, and a potential of −1.0 V was applied for 20 s relative to an external platinum counter/reference electrode using an EmStat potentiostat (PalmSens BV, Utrecht, the Netherlands). When complete, the exposed region of each electroanalysis electrode was coated with silver (circles) or gold (squares). The quality of the devices was evaluated after each stage using a Leica DM2000 optical microscope (Canada).

Device assembly and operation

Devices were assembled with an ITO-glass top-plate and a chromium-glass bottom-plate separated by a spacer formed from two pieces of Scotch double-sided tape (3 M, St. Paul, MN) with total spacer thickness of 180 μm. Unit droplet volumes on these devices were ~800 nL.

Droplet movement and magnetic particle control were managed using a custom instrument developed in collaboration with Abbott Diagnostics, described in detail elsewhere.[28] Briefly, to move droplets, sine wave potentials (100–120 V_{RMS}, 10 KHz) were applied between the top plate (ground) and sequential electrodes on the exposed contact pads in the bottom plate *via* a Pogo pin electronic interface. To load reagents into reservoirs, aliquots were placed near the appropriate

electrodes adjacent to the gap between the bottom and top plates; upon application of driving potential, the aliquots were driven onto the device. Waste and unused reservoir fluids were removed with KimWipes (Kimberly-Clark, Irving, TX). Unit droplets were dispensed from reservoirs by actuating a series of adjacent electrodes as described previously.[35] To perform an active mixing operation, a unit droplet was shuttled in a circular motion across four electrodes; more electrodes were used for larger droplets. Droplet actuation was monitored and recorded by a webcam. Magnetic particle position was controlled *via* a motor driven magnet beneath the device, in one of two positions. As described previously,[28] when operated in "standard" position, the magnet is positioned 3.6 cm below the device, which allows for the manipulation of droplets containing suspended particles. When operated in "separation" position, the magnet is positioned 150 μm below the device, such that particles become immobilized on the surface and droplets can be driven away. In a later step, particles that have been separated can be resuspended in a fresh droplet by returning the magnet to standard position. This process was used for all particle separation/resuspension steps described below.

DMF electroimmunoassay protocol

Prior to analysis, 5.0 μL aliquots of Ab_1 microparticle suspension, TSH sample solution, wash buffer, Ab_2–HRP solution (0.4 μg mL^{-1}), TMB solution, H_2O_2 solution, and stop solution were loaded into reservoirs on a device with 0.6 mm diameter gold working electrodes on the top plate. An eight-step protocol was used to effect immunoassays. (1) A unit droplet of Ab_1 microparticle suspension was dispensed from a reservoir and the particles were separated. (2) Five unit droplets of TSH were dispensed in three steps (2 droplets + 2 droplets + 1 droplet), and were consecutively delivered to the immobilized particles to be actively mixed for 3 min to resuspend the particles. The particles were then magnetically separated from the supernatant droplet, which was delivered to waste. (3) The particles were resuspended in four successive unit droplets of wash buffer (30 s of active mixing) and then separated again (with all supernatant droplets driven to waste). (4) Five unit droplets of Ab_2–HRP were dispensed in three steps (2 droplets + 2 droplets + 1 droplet), and were consecutively delivered to the immobilized particles to be actively mixed for 3 min to resuspend the particles. The particles were then magnetically separated from the supernatant droplet which was driven to waste. (5) Step 3 was repeated. (6) One unit droplet each of TMB and H_2O_2 solutions was dispensed and mixed. The combined droplet was delivered to the immobilized particles for resuspension and active mixing for 10 min and then separated, keeping the supernatant droplet. (7) One unit droplet of stop solution was dispensed and merged with the supernatant droplet for active mixing for 1 min. (8) The combined droplet was moved to the sensing electrodes on top-plate for electroanalysis. In typical analyses, the eight-step protocol was run in parallel to process one sample and one blank (five droplets each as in step 2), simultaneously. In step 8, the blank was measured first, followed by the sample, using the same WE and CE/RE.

Electroanalysis

Electroanalysis was used for three applications, all using an Emstat potentiostat: (1) to characterize the patterned electroanalysis electrodes, (2) to characterize detector response to immunoassay reagents, and (3) to detect the products of on-chip heterogeneous immunoassays. In the first application, a 20 μL aliquot of 1 mM $K_3Fe(CN)_6$ in McIlvaine's buffer (pH 7) was positioned on the patterned electroanalysis electrodes for characterization by cyclic voltammetry at scan rates of 20–200 mV s^{-1}. Five complete cycles were run for each scan rate. In the second application, a 1 : 1 mixture of Ab_2–HRP solution (at 0.02, 0.05, 0.1, 0.2, 0.5, and 1 μg mL^{-1}) and TMB–H_2O_2 solution was allowed to react for 2, 5, 10, or 15 min prior to reacting with one equivalent of stop solution. A 20 μL aliquot of the resulting solution was positioned on the electroanalysis electrodes (with 0.6, 0.8, 1.0 or 1.6 mm diameter Au WE) for analysis by amperometry at +0.15 V for 50 s, and the current value at 10 s was recorded for analysis. Three replicates were evaluated for each condition. In the third application, merged droplets of assay supernatant and stop solution in step 8 of the immunoassay protocol (2.4 μL, as above) were analyzed by amperometry at +0.15 V for 50 s and the current value at 10 s was recorded for analysis. Three replicates were evaluated for 0, 1, 2, 4, 8, and 20 μIU mL^{-1} TSH; a blank was run in parallel with each TSH sample. A background-corrected average response for each sample was calculated by subtracting the recorded current generated from the blank; these data were plotted as a function of concentration and were fitted to a linear least squares regression. The limit of detection (LOD) was defined as the regression value equal to three standard deviations of repeated blank measurements divided by slope.

Results and discussion

Device and detector

The goal of this work was to develop a digital microfluidic system for implementing immunoassays with integrated electrochemical analysis. There are only a few reports of DMF systems that have been used for electroanalysis,[30–34] and of these papers, only Dryden *et al.*[34] describes a fully automated analytical method including integrated electroanalysis electrodes, reagent dispensing and mixing, robust electrochemical characterization, and quantitative analysis. But a complicating factor for the Dryden *et al.* method[34] is the use of analysis electrodes embedded in the device bottom plate. DMF device bottom plates are crowded with an array of driving electrodes coated by an insulator; formation of electroanalysis electrodes (which should not be covered by an insulator) on the same substrate requires several extra fabrication steps. In this work we chose instead to position the analysis electrodes on the device top plate, which has no

insulator and is not crowded. In this, we joined an emerging trend of using DMF top plates as a useful position for adherent cell culture,[12,13] surface plasmon resonance (SPR) sensors,[14,16] and nucleation sites for crystal growth.[36]

The top plate in a digital microfluidic device is typically formed from a rigid substrate covered with conductive, transparent, indium tin oxide (ITO) and a fluorocarbon coating (often Teflon-AF). In standard DMF, the ITO on the top plate serves as a contiguous counter-electrode for droplet movement.[8] Here, as shown in Fig. 1a, we patterned the ITO on the top plate such that it serves two purposes: (1) the majority of the substrate is covered by a counter-electrode for DMF droplet actuation (as in typical systems); but (2) there are six isolated regions that serve as electroanalysis electrodes. As shown in Fig. 1b, working electrodes (WE) and counter/reference electrodes (CE/RE) were defined by electroplating gold in circle-shapes and silver in square-shapes on top of the designated ITO regions developed by a Teflon-AF lift-off process.[11] As shown in Fig. 1c, the completed top plate presents a surface that is primarily Teflon-AF, with small islands of exposed Au or Ag for electroanalysis. When paired with bottom plates to form complete DMF devices, droplets were observed to move efficiently and rapidly with no obvious differences relative to devices without patterned electroanalysis electrodes.

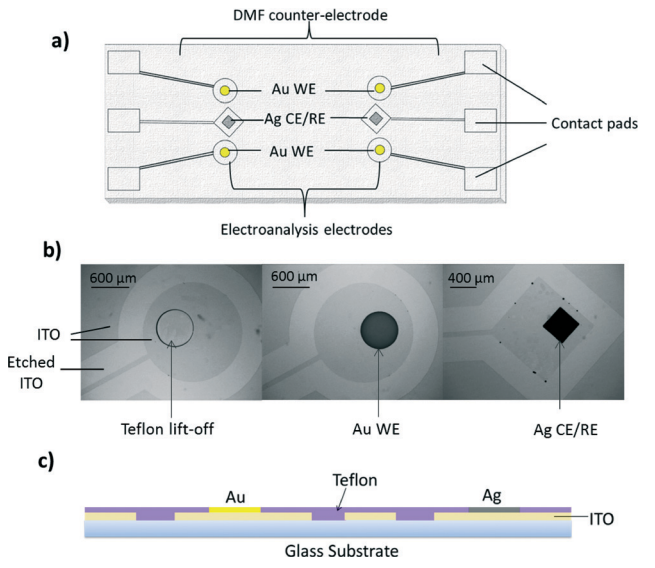

Fig. 1 Hybrid digital microfluidic device top-plate and electroanalysis system. a) Top-view schematic of top plate with six electroanalysis electrodes and one DMF counter-electrode. The six electroanalysis electrodes were defined as working electrodes (WE) or counter/reference electrodes (CE/RE) by electroplating with gold or silver, respectively, through apertures formed by a Teflon-AF lift-off process. b) Optical microscopic images of a Teflon lift-off spot prior to electroplating (left), an electroplated gold working electrode (middle), and a silver counter/psuedoreference electrode (right). The radius of the gold electrode (WE) is 300 μm and the side length of the silver electrode (CE/RE) is 400 μm. c) Side-view schematic of completed top plate, which is globally coated with Teflon-AF, punctuated with small islands of gold or silver.

In designing the system shown in Fig. 1, we evaluated numerous alternative strategies, including the use of bare ITO to form the electroanalysis electrodes. ITO is an established material for electrochemistry[37] which can be modified with self-assembled organic monolayers[38,39] or metal nanoparticles,[40,41] permitting its use in numerous applications. But in initial experiments with $Fe(CN)_6^{3-}$ in McIlvaine's buffer (pH 7) (data not shown), DMF top plates bearing bare ITO electrodes used for electroanalysis generated low current. This behavior was attributed to the high affinity of phosphate anions in the buffer, which inhibits the adsorption of negatively charged ferricyanide redox probes onto the ITO surface.[37] In addition to low current, the signal from ITO electrodes was noisy and unstable when used with immunoassay reagents, perhaps because of the complex nature of the matrix. Thus, in the methods reported here, we used gold (WE) and silver (CE/RE) electroanalysis electrodes (as in Fig. 1). When applied to electroanalysis, these devices were stable over the course of many measurements, and could be used several weeks after preparation with no loss of signal.

The electrochemical performance of the new hybrid DMF–electroanalysis system was characterized using cyclic voltammetry (CV). Fig. 2a shows representative CV results for 1 mM $Fe(CN)_6^{3-}$ in McIlvaine's buffer (pH 7) at scan rates of 20–200 mV s^{-1}. The separation between cathodic and anodic peak potentials is $\Delta E_p \approx 130$ mV/n (where n is the number of moles of electrons transferred). This behaviour is similar to that of commercially available screen printed electrodes for which $\Delta E_p \approx 100$ mV/n (data not shown). More importantly, the new system exhibits reversible behavior as predicted by the Randles–Sevcik equation,[42] $i_p = (2.69 \times 10^5)AC_iD^{1/2}v^{1/2}n^{3/2}$, where i_p is peak current, A is the area of the electrode, C_i is the concentration of the electroactive species, D is the diffusion coefficient, and v is the scan rate. According to this expression, $i_p \propto v^{1/2}$, which can be seen in Fig. 2b. Regression lines fit to these data resulted in equations of $y = 0.0561x - 0.0896$ with $R^2 = 0.9911$ for positive peak currents and $y = -0.0538x + 0.0541$ with $R^2 = 0.9975$ for negative peak currents, respectively. Finally, when cyclic voltammograms of $Fe(CN)_6^{3-}$ were collected from different hybrid DMF–electroanalysis devices ($n = 4$), the current response variation was 6.8% RSD. This variance is likely a function of slight differences in electrode size caused by imperfect Teflon-AF lift-off fidelity.

System characterization for immunoassay reagents

The most common electrochemical detection technique in immunoassays is amperometry,[43,44] which is performed in a diffusion-controlled regime of mass transport on electrode surfaces. The use of sensing electrodes with small dimensions improves assay sensitivity by shifting from planar to non-planar diffusion, leading to efficient transport of electroactive species to the transducer surface. This in turn increases the signal-to-noise ratio, and thus improves the

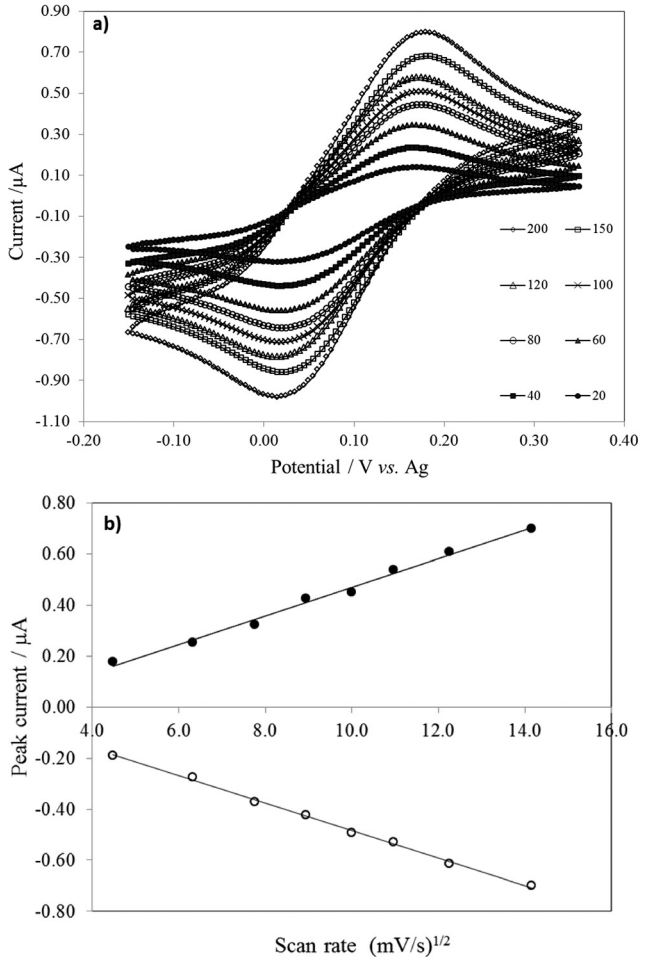

Fig. 2 Electrochemical characterization of hybrid DMF–electroanalysis system. a) Cyclic voltammograms of 1 mM $Fe(CN)_6^{3-}$ in McIlvaine's buffer (pH 7) on 300 μm radius Au WE relative to Ag CE/RE at 20 (●), 40 (■), 60 (▲), 80 (○), 100 (×), 120 (Δ), 150 (□), and 200 mV s^{-1} (◊). b) Randles–Sevcik plot of positive (●) and negative (○) peak currents as a function of the square root of scan rate.

limit of detection in low concentration regimes. We hypothesized that the system described here would be useful for amperometric detection of immunoassay reaction products with comparable performance to those described previously, with sensitivity adequate for detecting small amounts of analyte in microfluidic samples.

Building from previous work,[45,46] an amperometric detection system was developed that relies on the action of the enzyme, horseradish peroxidase (HRP), on the substrate, 3,3′,5,5′-tetramethylbenzidine (TMB), in the presence of H_2O_2. This reaction generates a blue intermediate which turns yellow upon termination of the reaction by acidification. The yellow product has been identified as a positively charged two-electron oxidation product (a diimine), which is suitable for detection by amperometry.[47] Prior to implementing heterogeneous DMF-driven immunoassays, the response of the new system to the key reaction components was characterized (without droplet movement) using a homogeneous reaction between an antibody–enzyme conjugate (Ab_2–HRP), TMB, and H_2O_2. After reacting for a given incubation period, the assay was acidified and the products were interrogated using the top-plate detector.

Typical amperometric responses of the system for the homogeneous HRP–TMB–H_2O_2 reaction are depicted in Fig. 3a; as shown, the amperometric current response stabilizes in 10–30 s, and the absolute current values decrease as a function of increasing Ab_2–HRP concentration. Fig. 3b is a plot of current magnitude (measured at 10 s) as a function of Ab_2–HRP concentration. As shown, the current response increases as a function of Ab_2–HRP concentration to a maximum for 0.5 μg mL^{-1}; however, a further increase in Ab_2–HRP concentration to 1 μg mL^{-1} resulted in decreased current, which may be the result of surface fouling. Current magnitudes as a function of incubation time and working electrode radius are shown in Fig. 3c and d, respectively. As shown, the current magnitude is higher for increased time and electrode size; however, the increase in detector response is associated with a concomitant increase in measurement error. Thus, an incubation time of 10 min and WE radius of 300 μm were chosen as a reasonable compromise between signal intensity and variance for all remaining experiments.

The homogeneous reaction used to generate the data shown in Fig. 3, in which Ab_2–HRP molecules are in solution, is not a perfect analogue for heterogeneous immunoassays in which Ab_2–HRP molecules are bound to magnetic beads (described in the following section). But these data are representative of the electroanalytical response of this system for these reagents, and gave us a useful starting point for development of the fully integrated method. In general terms, the performance of the electroanalytical sensor reported here (600 μm dia. WE, ~40 nA) is comparable previously reported macroelectrode systems (3 mm dia. WE, 500 nA) applied to the same electrochemical reaction.[45]

DMF electroimmunoassays

As described in the introduction, there is great enthusiasm for the miniaturization of immunoassays in the digital microfluidic format; however, all of the methods reported previously have relied on optical detection.[22–28] In developing the first digital microfluidic immunoassay with integrated electrochemical detection, we chose thyroid stimulating hormone (TSH) as a test-case, motivated by the importance of this marker in clinical testing for thyroid disease.[48] A heterogeneous DMF electroimmunoassay for TSH was developed, which is depicted in Scheme 1. Droplets bearing samples, reagents, and magnetic beads are sandwiched between a bottom plate bearing driving electrodes and a top plate bearing electroanalysis electrodes. TSH molecules are captured by primary antibodies (Ab_1) on magnetic particles, which are then used to capture secondary antibody conjugates (Ab_2–HRP), which are in turn used to catalyze the formation of oxidized substrate (TMB^+) for amperometric detection. Note that this scheme was designed for droplets suspended in air rather than the more common format in which droplets are

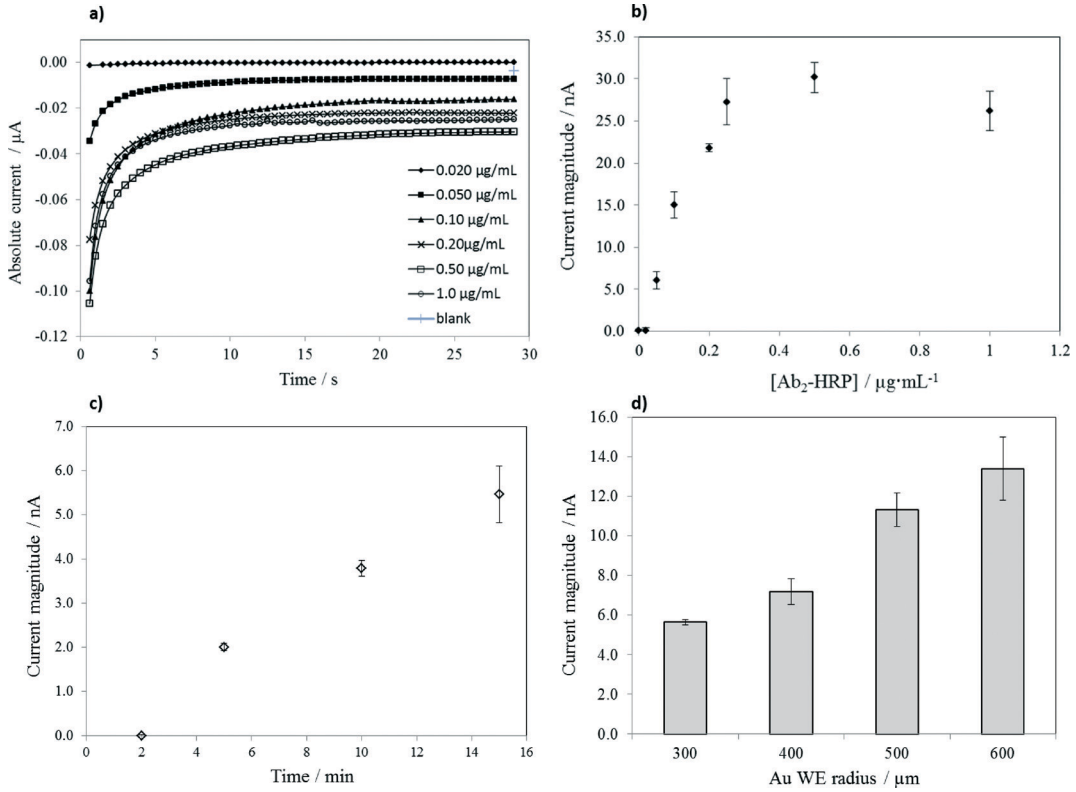

Fig. 3 Characterization of the hybrid DMF–electroanalysis system for a homogeneous HRP–TMB–H_2O_2 reaction with +0.15 V applied to the Au WE relative to the Ag CE/RE. a) Typical absolute amperometric current responses after 10 min incubation with substrate, measured on top plate with 300 μm radius WE for blank (|), 0.020 (♦), 0.050 (■), 0.10 (▲), 0.20 (×), 0.50 (□) and 1.0 (○) μg mL^{-1} Ab_2–HRP. b) Reactions (and replicates) from a) plotted as current magnitude as a function of Ab_2–HRP concentration. c) Plot of current magnitude as a function of incubation time for 0.1 μg mL^{-1} Ab_2–HRP measured on top plate with 300 μm radius WE. d) Bar graph of current magnitude as a function of Au WE radius for 0.05 μg mL^{-1} Ab_2–HRP after 10 min incubation. Error bars are ±1 S.D.

suspended in oil.[23–25,27] We propose that device formats requiring oil would be incompatible with the electroanalytical techniques reported here, as oil would likely foul the electrode surfaces.

Fig. 4a depicts a hybrid DMF–electroanalysis device. Many variations in buffer constituents and reagent concentration were evaluated to obtain an immunoassay procedure compatible with reliable droplet movement, acceptable enzyme and antibody activity, and adequate electroanalytical sensitivity. For example, as described previously,[26] care must be taken to select surfactants that are compatible with DMF droplet actuation in air. The final, optimized eight-step procedure is described in detail in the experimental section. The procedure includes a sequence of magnetic particle separations (Fig. 4b–e), reagent deliveries and particle resuspensions (Fig. 4f & g), and particle washes. The final step of the procedure is delivery of a droplet containing acidified, oxidized TMB^+ to one of the electroanalytical cells on the top plate (Fig. 4h). As shown, this droplet spans the gap between the WE and one of the CE/REs. Each TSH sample analysis is

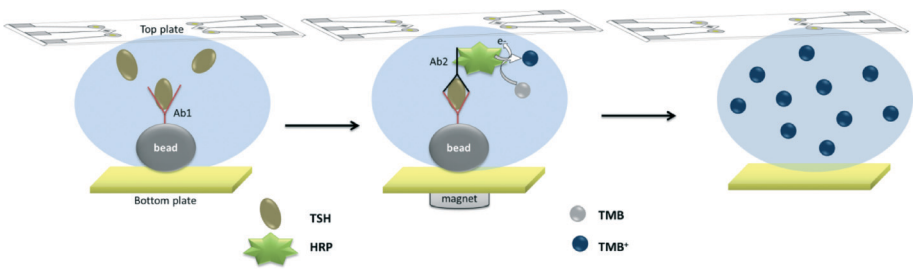

Scheme 1 Schematic (not to scale) depicting key steps in the DMF electroimmunoassay. First (left panel), magnetic particles conjugated with primary antibody (Ab_1) trap thyroid stimulating hormone (TSH) antigen molecules in the sample droplet. Second (middle panel), secondary antibody conjugated with horseradish peroxidase enzyme (Ab_2–HRP) is bound to the immobilized antigen in sandwich format, which is mixed with the substrate (TMB). Third (right panel), oxidized substrate molecules (TMB^+) are detected amperometrically on the hybrid DMF top-plate–electroanalysis system.

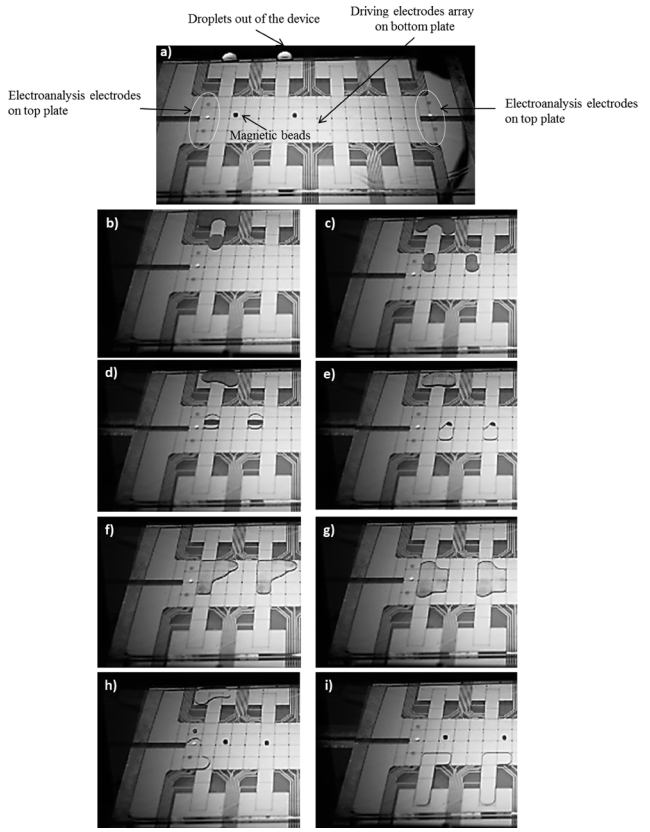

Fig. 4 Digital microfluidic electroimmunoassay. a) Complete device featuring a top plate (mostly transparent but with visible Au/Ag electroanalysis electrodes on the left and right) and a bottom plate bearing an array of driving electrodes. In b), a droplet containing Ab_1-labeled microparticles is driven onto the device. In c), a second droplet of labeled microparticles joins the first, allowing for two immunoassays to run simultaneously. In d & e), the magnet is engaged, allowing for the separation of the magnetic particles (on the bottom-plate surface) from the supernatant (driven to waste reservoirs). In f & g), droplets of sample are dispensed, merged, and then mixed to homogeneously resuspend the particles. After several additional steps (delivery of Ab_2–HRP, delivery of TMB–H_2O_2, *etc.*), in h), the droplet containing the final product of the immunoassay is driven to the electroanalysis electrodes on the top plate, highlighted in a white circle. Finally, in i), after analysis by amperometry, droplets are moved to waste.

coupled with a blank analysis to allow for background subtraction, and after current magnitude measurements, the droplets are moved to waste (Fig. 4i), and the system is reset for another assay.

Using the protocol described above, a calibration curve was generated for TSH detection (Fig. 5). A regression line was fit to the data ($y = 0.4316x + 1.3477$, $R^2 = 0.995$), and the LOD was determined to be 2.4 μIU mL^{-1}. This LOD is higher than those reported previously for TSH immunoassays relying on chemiluminescence detection,[26,28] but it is comfortably lower than the clinical cut-off value for diagnosis of thyroid disease: 3.0 μIU mL^{-1}.[49] Moreover, the potentiostat used in this study is very compact ($2.25 \times 1.5 \times 1$ in^3), which suggests that this technique may be a good fit for portable diagnostics. If greater sensitivity is needed in future applications,

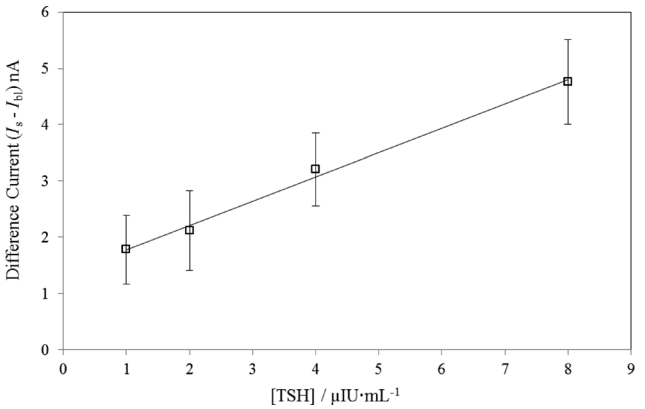

Fig. 5 Calibration curve for the DMF electroimmunoassay. The difference between the absolute current response of each TSH concentration and a blank current measurement is plotted as a function of TSH concentration. Each concentration was evaluated in triplicate, and error bars are ±1 S.D.

potential solutions include the use of 3D nanostructures on electrode surfaces[50] or comprehensive blocking of non-specific adsorption onto the capture surface.[51]

Conclusion

Here, we introduce the first digital microfluidic immunoassay relying on electrochemical detection. In this system, electrodes were integrated onto an etched ITO-glass substrate by direct electrodeposition on Teflon lift-off sites. This hybrid device successfully performs dual functions: droplet movement and electrochemical detection. The system was successfully applied to implementing TSH immunoassays with a detection limit of 2.4 μIU mL^{-1}. We propose that the compact size of this detector will make this type of system attractive for portable analysis, such as point-of-care diagnostics.

Acknowledgements

We thank the Canadian Institutes for Health Research (CIHR), the National Science and Engineering Research Council (NSERC), and Abbott Diagnostics for financial support. We thank Prof. Shana Kelley (Univ. Toronto) for advice. A.H.C.N. thanks NSERC for a graduate fellowship, and A.R.W. thanks the Canada Research Chair (CRC) Program for a CRC.

References

1 M. Abdelgawad and A. R. Wheeler, *Adv. Mater.*, 2009, **21**, 920–925.
2 E. M. Miller and A. R. Wheeler, *Anal. Bioanal. Chem.*, 2009, **393**, 419–426.
3 M. J. Jebrail and A. R. Wheeler, *Curr. Opin. Chem. Biol.*, 2010, **14**, 574–581.
4 M. G. Pollack, V. K. Pamula, V. Srinivasan and A. E. Eckhardt, *Expert Rev. Mol. Diagn.*, 2011, **11**, 393–407.
5 S. K. Cho and H. Moon, *BioChip J.*, 2008, **2**, 79–96.

6 L. Malic, D. Brassard, T. Veres and M. Tabrizian, *Lab Chip*, 2010, **10**, 418–431.
7 A. R. Wheeler, *Science*, 2008, **322**, 539–540.
8 K. Choi, A. H. C. Ng, R. Fobel and A. R. Wheeler, *Annu. Rev. Anal. Chem.*, 2012, **5**, 413–40.
9 I. Barbulovic-Nad, H. Yang, P. S. Park and A. R. Wheeler, *Lab Chip*, 2008, **8**, 519–526.
10 I. Barbulovic-Nad, S. Au and A. R. Wheeler, *Lab Chip*, 2010, **10**, 1536–1542.
11 I. Eydelnant, U. Uddayasankar, B. Li, M. Liao and A. Wheeler, *Lab Chip*, 2012, **12**, 750–757.
12 S. Srigunapalan, I. Eydelnant, C. Simmons and A. Wheeler, *Lab Chip*, 2012, **12**, 369–375.
13 D. Bogojevic, M. Chamberlain, I. Barbulovic-Nad and A. Wheeler, *Lab Chip*, 2012, **12**, 627–634.
14 L. Malic, T. Veres and M. Tabrizian, *Biosens. Bioelectron.*, 2009, **24**, 2218–2224.
15 Y.-J. Liu, D.-J. Yao, H.-C. Lin, W.-Y. Chang and H.-Y. Chang, *J. Micromech. Microeng.*, 2008, **18**, 1–7.
16 L. Malic, T. Veres and M. Tabrizian, *Lab Chip*, 2009, **9**, 473–475.
17 V. N. Luk and A. R. Wheeler, *Anal. Chem.*, 2009, **81**, 4524–4530.
18 D. Chatterjee, A. J. Ytterberg, S. U. Son, J. A. Loo and R. L. Garrell, *Anal. Chem.*, 2010, **82**, 2095–2101.
19 H. Moon, A. R. Wheeler, R. L. Garrell, J. A. Loo and C. J. Kim, *Lab Chip*, 2006, **6**, 1213–1219.
20 A. R. Wheeler, H. Moon, C. A. Bird, R. R. Loo, C. J. Kim, J. A. Loo and R. L. Garrell, *Anal. Chem.*, 2005, **77**, 534–540.
21 A. R. Wheeler, H. Moon, C. J. Kim, J. A. Loo and R. L. Garrell, *Anal. Chem.*, 2004, **76**, 4833–4838.
22 E. M. Miller, A. H. Ng, U. Uddayasankar and A. R. Wheeler, *Anal. Bioanal. Chem.*, 2011, **399**, 337–345.
23 R. S. Sista, A. E. Eckhardt, V. Srinivasan, M. G. Pollack, S. Palanki and V. K. Pamula, *Lab Chip*, 2008, **8**, 2188–2196.
24 R. Sista, Z. Hua, P. Thwar, A. Sudarsan, V. Srinivasan, A. Eckhardt, M. Pollack and V. Pamula, *Lab Chip*, 2008, **8**, 2091–2104.
25 N. Vergauwe, D. Witters, F. Ceyssens, S. Vermeir, B. Verbruggen, R. Puers and J. Lammertyn, *J. Micromech. Microeng.*, 2011, **21**, 054026.
26 A. H. C. Ng, K. Choi, R. P. Luoma, J. M. Robinson and A. R. Wheeler, *Anal. Chem.*, 2012, **84**, 8805–8812.
27 S. Emani, R. Sista, H. Loyola, C. C. I. Trenor, V. K. Pamula and S. M. Emani, *Blood Coagulation Fibrinolysis*, 2012, **23**, 760–768.
28 K. Choi, A. H. C. Ng, R. Fobel, D. A. Chang-Yen, L. E. Yarnell, E. L. Pearson, C. M. Oleksak, A. T. Fischer, R. P. Luoma, J. M. Robinson, J. Audet and A. R. Wheeler, *Anal. Chem.*, 2013, **85**, 9638–9646.
29 F. Riccia, G. Adornettoa and G. Palleschia, *Electrochim. Acta*, 2012, **84**, 74–83.
30 P. Dubois, G. Marchand, Y. Fouillet, J. Berthier, T. Douki, F. Hassine, S. Said Gmouh and M. Vaultier, *Anal. Chem.*, 2006, **78**, 4909–4917.
31 J. L. Poulos, W. C. Nelson, T.-J. Jeon, C.-J. Kim and J. J. Schmidt, *Appl. Phys. Lett.*, 2009, **95**, 013706.
32 C. Karuwan, K. Sukthangb, A. Wisitsoraata, D. Phokharatkula, V. Patthanasettakula, W. Wechsatolb and A. Tuantranont, *Talanta*, 2011, **84**, 1384–1389.
33 T. Lederer, S. Clara, B. Jakoby and W. Hilber, *Microsyst. Technol.*, 2012, **18**, 1163–1180.
34 M. D. M. Dryden, D. D. G. Rackus, M. H. Shamsi and A. R. Wheeler, *Anal. Chem.*, 2013, **85**, 8809–8816.
35 S. K. Cho, H. J. Moon and C. J. Kim, *J. Microelectromech. Syst.*, 2003, **12**, 70–80.
36 D. Witters, N. Vergauwe, R. Ameloot, S. Vermeir, D. De Vos, R. Puers, B. Sels and J. Lammertyn, *Adv. Mater.*, 2012, **24**, 1316–1320.
37 G. Xu, Y. Iwasaki and O. Niwa, *Chem. Lett.*, 2005, **34**, 1120–1121.
38 T. J. Gardner, C. D. Frisbie and M. S. Wrighton, *J. Am. Chem. Soc.*, 1995, **117**, 6927–6933.
39 S.-Y. Oh, Y.-J. Yun, D.-Y. Kim and S.-H. Han, *Langmuir*, 1999, **15**, 4690–4692.
40 X. Dai and R. Compton, *Anal. Sci.*, 2006, **22**, 567–570.
41 N. Sakai, Y. Fujiwara, M. Arai, K. Yu and T. Tatsuma, *J. Electroanal. Chem.*, 2009, **628**, 7–15.
42 A. J. Bard and L. R. Faulkner, *Electrochemical Methods: Fundamentals and Applications*, 2nd edn, John Wiley and Sons Publishers, 2001.
43 G. Volpe, U. Sozzo, S. Piermarini, E. Delibato, G. Palleschi and D. Moscone, *Anal. Bioanal. Chem.*, 2013, **405**, 655–663.
44 F. Ricci, A. Amine, D. Moscone and G. Palleschi, *Biosens. Bioelectron.*, 2007, **22**, 854–862.
45 G. Volpe, D. Compagnone, R. Draisci and G. Palleschi, *Analyst*, 1998, **123**, 1303–1307.
46 P. Fanjul-Bolado, M. B. González-García and A. Costa-García, *Anal. Bioanal. Chem.*, 2006, **386**, 1849–1854.
47 P. D. Josephy, T. Eling and R. P. Mason, *J. Biol. Chem.*, 1982, **257**, 3669–3675.
48 B. Biondi and D. S. Cooper, *Endocr. Rev.*, 2008, **29**, 76–131.
49 L. Wartofsky and R. A. Dickey, *J. Clin. Endocrinol. Metab.*, 2005, **90**, 5483–5488.
50 L. Soleymani, Z. Fang, E. H. Sargent and S. O. Kelley, *Nat. Nanotechnol.*, 2009, **4**, 844–848.
51 D. Huber, J. Rudolf, P. Ansari, B. Galler, M. Fuhrer, C. Hasenhindl and S. Baumgartner, *Anal. Bioanal. Chem.*, 2009, **394**, 539–548.

